Japanese Journal of Applied Physics

REGULAR PAPER

Fabrication of Si photonic waveguides by electron beam lithography using improved proximity effect correction

Japanese Journal of Applied Physics **59**, 126502 (2020) **REGULAR PAPER**
https://doi.org/**10.35848/1347-4065/abc78d**

Fabrication of Si photonic waveguides by electron beam lithography using improved proximity effect correction

Moataz Eissa[1*], Takuya Mitarai[1], Tomohiro Amemiya[1,2], Yasuyuki Miyamoto[1,2], and Nobuhiko Nishiyama[1,2]

[1]*Department of Electrical and Electronic Engineering, Tokyo Institute of Technology, Meguro, Tokyo 152-8552, Japan*
[2]*Laboratory for Future Interdisciplinary Research of Science and Technology (FIRST), Institute of Innovative Research (IRR), Tokyo Institute of Technology, Meguro, Tokyo 152-8552, Japan*

[*]E-mail: eissa.m.aa@m.titech.ac.jp

Received July 8, 2020; revised October 14, 2020; accepted November 3, 2020; published online November 20, 2020

In this work, electron beam lithography proximity effect correction (PEC) was experimentally studied for patterning of Si photonic waveguides with a relatively thick resist mask. Beam's energy density distribution (EDD) was experimentally extracted by the line exposure method; however, exposure lines in this work were developed after cleavage with a high-contrast process to reduce developer-related effects. The measured line spread function was fitted to a 4-Gaussian function to model mid-range energy densities accurately. The extracted EDD showed less proximity effects compared to conventional Monte-Carlo simulation performed by a commercial software. PEC processes with both techniques were experimentally compared for a Si photonic waveguide pattern with different side-cladding trench widths. Microscopic images confirmed that the presented calibration method could achieve better development conditions near the required clearance dosage. Single-mode propagation loss for a 500 × 220 nm Si wire waveguide was reduced from 3.2 to 2.4 dB cm^{-1} using the presented process.

1. Introduction

Si photonics has been an active research field in the last decade due to its potential towards optoelectronics integration. Si optical devices can be integrated within a CMOS compatible process to yield high-performance Si chips, that offer optical functionalities with reduced cost.[1)] Hence, it can be a promising candidate to exceed the speed bottleneck for data interconnects.[2,3)] Si photonics platform is characterized by a high index contrast material system due to the relatively large difference of refractive indices between Si and SiO_2 in the silicon-on-insulator (SOI) chips, which allows high optical confinement in Si waveguides with silicon dioxide (SiO_2) cladding. This allows realization of compact devices with small footprints,[4,5)] and hence, integration density could be increased.

However, high optical confinement in Si photonics causes higher dependence of the device's performance on its dimensions. Hence, the reduction of fabrication tolerances is required to reduce the induced sensitivity.[6)] Moreover, process resolution,[7)] etching anisotropy,[8)] and sidewall roughness,[9)] significantly affect the performance of Si photonics devices and add more constraints to the fabrication process.[10)] A few R&D and pre-commercial facilities recently started processing of CMOS compatible Si photonics circuits using 300 mm wafer fabs by 193 nm immersion lithography.[11)] However, for R&D purposes, the state-of-the-art CMOS process has disadvantages such as high fabrication cost and long whole processing time. Therefore, electron beam lithography (EBL) is a suitable tool for this purpose.[12)] However, as the resist is exposed to the e-beam, forward-scattering, and backscattering of electrons are known to cause beam broadening[13)] and proximity effects,[14)] respectively. Hence, it is difficult to completely resolve different pattern densities by a fixed electron dose without the possible occurrence of over-development and significant resist under-cuts.[15)] Such under-cuts depend mainly on the surrounding pattern area density. Hence, the critical dimension (CD) uniformity and etching anisotropy are degraded accordingly.

As the device's characteristics are relatively sensitive to dimensional variations, reduction of fabrication tolerances becomes necessary in some applications to improve system performance. For telecom applications utilizing Si photonics, performance merits such as wavelength accuracy, polarization stability, and power loss strongly depend on the allowed lithography tolerance. For example, if we consider a dense wavelength division multiplexing (DWDM) system with 50 GHz ITU grid, less than 0.04 nm (5 GHz, 10% of the grid spacing) free spectral range variation may be required.[16)] To achieve this value, $<\pm 6$ nm tolerance in single-mode waveguide width is needed for a ~ 20 μm diameter ring-resonator filter. Moreover, vertical waveguide sidewalls with angles $> 88°$ are required to avoid optical mode hybridization at taper structures and bends especially for TM polarization.[8)] Propagation loss of the waveguide is also important when long waveguide sections are involved. For a Mach–Zehnder interferometer modulator with a typical full device length of 2 mm, achieving power loss of $<10\%$ requires a propagation loss of <2.3 dB cm^{-1}. To achieve the previously mentioned specifications by EBL, an improved proximity effect correction (PEC) method is proposed in this work to obtain better development conditions with vertical sidewalls, through accurate representation of the scattered electron beam.

2. EBL PEC process for Si photonics

In this work, a relatively thick ZEP-520A resist mask of 700 nm thickness was used for SOI chips with the standard 220 nm thick top Si. In order to simplify the patterning process, no intermediate hard mask layer was used. The resist thickness was chosen to be thick enough to compensate for Si dry-etching selectivity to the resist polymer, and hence, allow complete etching of the top Si layer. EBL was performed using a spot-beam scanning-type JEOL JBX-6300FS system operating at 50 kV acceleration voltage, 200 pA beam current, and 4 nm shot pitch. Exposed patterns were

developed by ZED-N50; the recommend high-resolution strong developer for ZEP resist.

As the electron beam scatters in the resist and substrate materials, beam broadening and proximity effects take place. Figure 1 shows a schematic view of both scattering effects. Such phenomena result in different development conditions for different pattern area densities at the same electron dosage. Unfortunately, different pattern area densities are usually encountered in Si photonics chips. For example, a single-mode high-confinement ~500 nm width Si waveguide pattern with ~1 μm side-cladding trench widths is tapered to a narrow ~220 nm width spot-size converter (SSC) with ~5 μm side-cladding trench widths to allow optical mode expansion and edge-coupling to a lensed optical fiber. Figure 2 shows microscopic images after development for such pattern at different fixed doses. It can be seen in Fig. 2(a) that a low dose of 170 μC cm^{-2} causes under-development for the narrower trench area. Although a higher dose of 225 μC cm^{-2} can develop that area as shown in Fig. 2(b), it may over-develop the pattern-dense SSC area and cause additional resist under-cuts that affect SSC's width. Such effects are caused mainly by the aforementioned electron scattering.

Therefore, PEC is usually used to achieve better development conditions and to control pattern's CD,[17] which is resist's bottom width in this case. Dose modulation PEC is a common technique where exposure dose is varied locally with respect to a reference dose called the base dose. Generally, the dose modulation PEC process is divided into two main steps. The first is to obtain the radial energy density distribution (EDD) of the electron beam, while the second is to apply a dose modulation algorithm. The algorithm defines a spatial grid for the pattern and assigns a local dose to each grid point according to beam's EDD and the surrounding pattern area density.

In our previous report, we reported the fabrication and measurement of Si-waveguides with dose modulation PEC for a 700 nm thick ZEP mask.[18] Conventional EDD representation was utilized, where beam energy distribution is simulated by the Monte-Carlo scattering simulation technique.[19] Simulation was performed using commercial software.[20] Then, EDD was obtained by 2D convolution with an extracted Gaussian process blur. Proximity effects

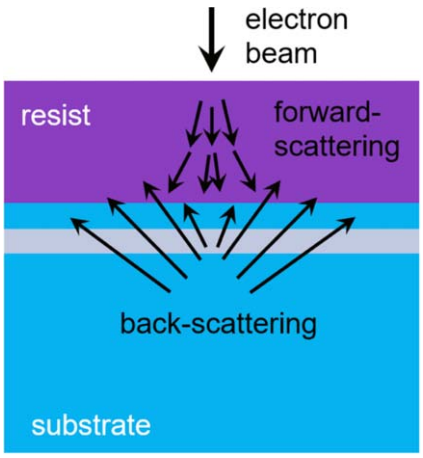

Fig. 1. (Color online) Forward-scattering and backscattering of electrons in the resist and substrate.

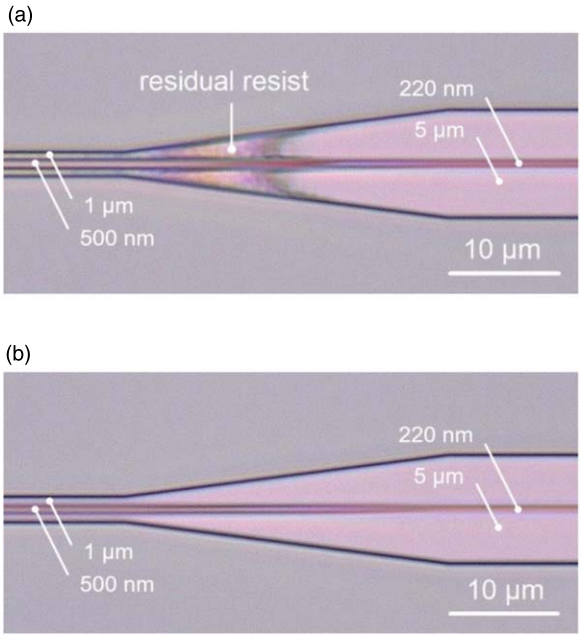

Fig. 2. (Color online) Si waveguide with 1 μm trench tapered to a 5 μm trench SSC developed after exposure with a fixed dose of (a) 170 μC cm^{-2} and (b) 225 μC cm^{-2}.

were corrected using another software[21] to fabricate Si photonics waveguide patterns. However, it was found that such a PEC method still shows pattern dependence, although it worked for some pattern densities.

In this work, we investigate techniques to achieve accurate PEC using our thick-resist process. Section 3 shows that a better representation of beam's EDD could be obtained experimentally using the well-known line exposure method[22] with two proposed improvements. The first improvement was to develop lines' cross-sections after cleavage in order to reduce developer penetration issues in narrow lines, while the second one was to use cold development in order to enhance process contrast and reduce developer-dependent chemical effects.[23] Section 4 shows the obtained results of PEC process calibration and Si photonics waveguide fabrication with different side-cladding trench widths.

3. Extraction of beam parameters

In literature, various methods were proposed to extract the radial dependence of the deposited energy density of the electron beam. A common approach is the point exposure method,[24] where a calibration pattern of isolated points with various doses is exposed and developed. Then, pattern radii are measured and plotted against the corresponding inverse doses to directly obtain the radial EDD. It is important to note that resist dimensions are usually different at the top and the bottom due to the under-cuts caused by backscattering effects especially at radii corresponding to near-mid- or short-ranges where pattern dimensions are comparable to or smaller than the resist thickness, respectively. Here, it is more convenient to extract EDD at the bottom of the resist. The CD to be controlled by PEC in dry etching applications is chosen to be the bottom width to achieve vertical resist sidewalls and hence anisotropic etching. Since measurement of the developed pattern radii is usually performed by top observation

using a scanning electron microscope (SEM), the measurement of resist's bottom dimensions is difficult in that calibration approach. Moreover, it is also difficult to accurately characterize short-range energy densities where pattern dimensions are comparable to the effective beam radius or process resolution; since developer penetration issues or loading, effects may be encountered for such small radii. Therefore, other indirect methods were proposed in the literature to characterize short-range scattering effects and estimate the short-range scattering parameter.[25)]

Another similar approach for extracting EDD is the line exposure method, where long-isolated lines with various doses are exposed, developed, and measured from the side by cross-sectional observation. Developed bottom half-widths can be plotted versus the corresponding inverse doses to obtain the energy spread function of the exposed lines. From a mathematical perspective, the line spread function (LSF) is simply a convolution between the point spread function (PSF) and an infinitely long line.[26)] The radial EDD can be estimated then by deconvolution of LSF with a long line. The main advantage of the line exposure method is that cross-sectional observation is possible, hence, various exposure and development behaviors across the resist cross-section can be extracted.[27)]

Although the conventional LSF method enables EDD estimation at the resist bottom in contrast to the LSF one, it still suffers from some similar drawbacks. It is still not immune to the developer-related issues previously mentioned, especially for relatively thick resists. Extraction of short-range energy distribution still suffers from accuracy issues since developer penetration in narrow line grooves would be more difficult than wider ones. Moreover, development processes used in literature for calibration were usually similar to those used for the original fabrication processes that did not necessarily have very high contrast values.[25)] Actually, the previously discussed point and line exposure methods assume a simple threshold model for the development process, which in turn assumes an infinite contrast to neglect non-ideal developer effects.[27)] Therefore, a lower contrast of the development process can lead to less accurate extraction of the LSF, as developer effects will be embedded in the measured line half-widths. Strictly speaking, a development model should be utilized to consider such developer effects. Thus, a dedicated resist with very high contrast was used in early work to propose the point exposure method assuming a simple threshold model.[24)]

In this section, techniques towards the improvement of the line exposure method by reduction of such developer effects are proposed and discussed so that the assumption of a threshold development model could be rather more valid. In the next section, the proposed experimental technique is compared with the conventional one that represents EDD by convolution of a PSF obtained by Monte-Carlo simulation with a Gaussian beam blur.

3.1. Cross-section direct development after cleavage

In the conventional line exposure method, the exposed line pattern is developed firstly and then the chip is cleaved for cross-sectional observation. However, such a pattern development technique suffers from developer penetration issues in narrow line grooves as mentioned before. Therefore, we propose an improved technique where development is performed after chip cleavage. Hence, the developer can interact directly with the resist cross-section and develop narrow line grooves without penetration issues. Pattern development loading effects can be neglected if a strong developer is used. This technique was applied to extract EDD for our SOI EBL process. A set of area doses equally spaced in the logarithmic scale ranging from 6.31×10^3 to 2.5×10^7 μC cm^{-2} was assigned to a set of long-isolated lines exposed to the 700 nm thick ZEP resist with a

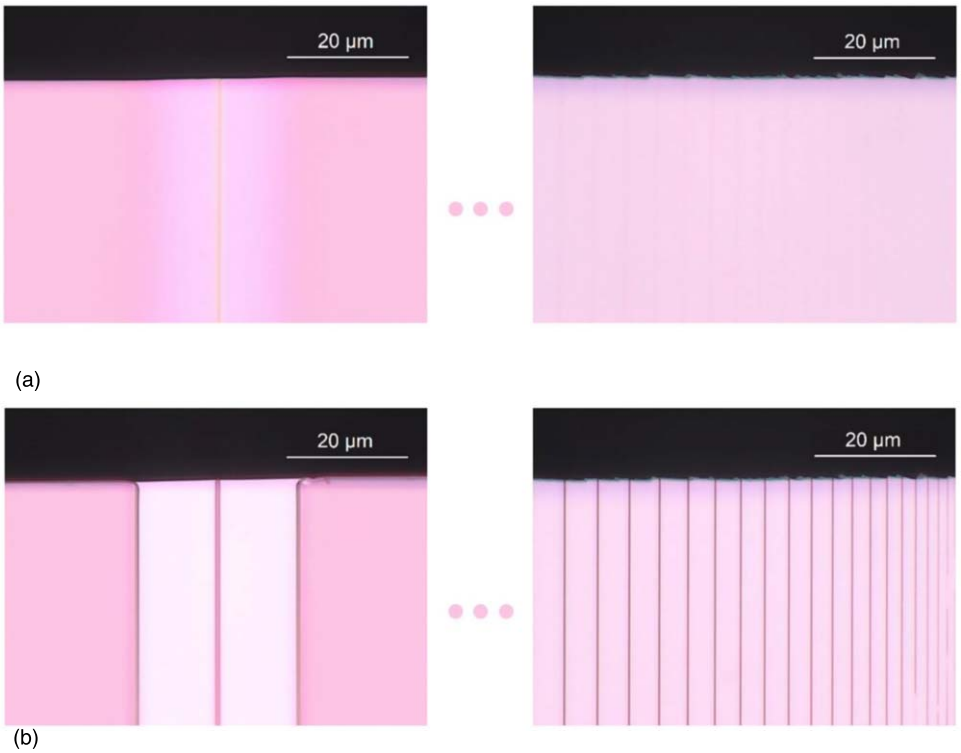

Fig. 3. (Color online) Microscopic images (top observation) of the LSF calibration pattern: (a) line exposure and cleavage, and (b) line development.

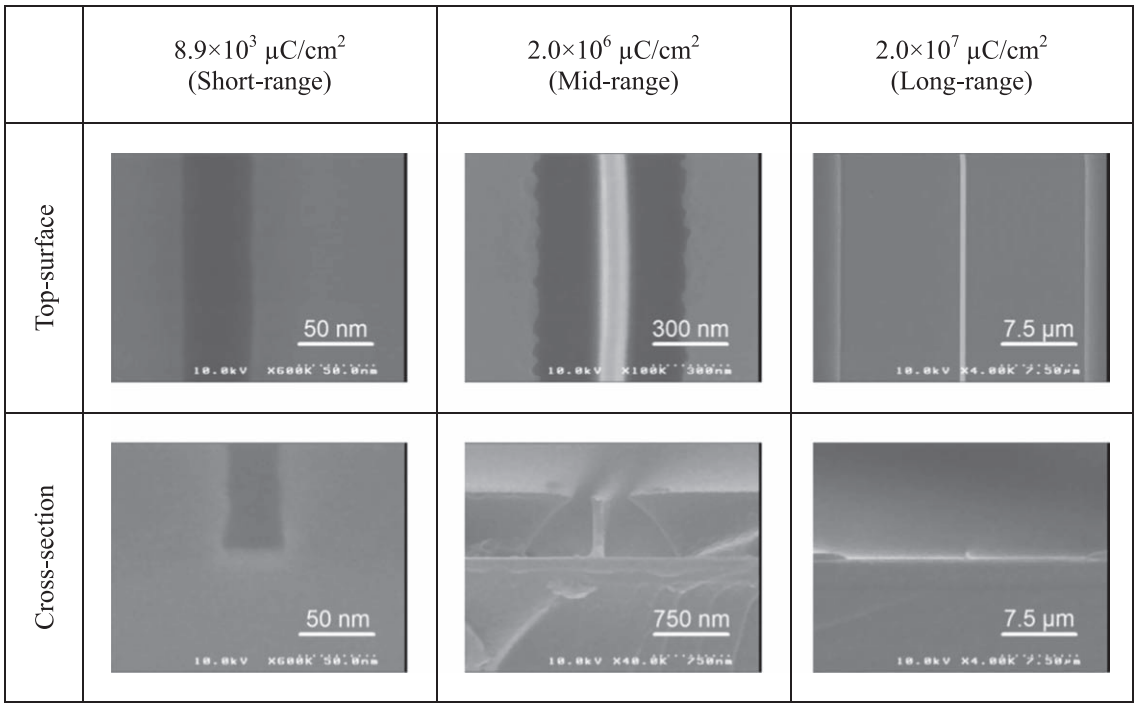

Fig. 4. SEM image samples for line half-width observation at the top and bottom resist surfaces for different scattering ranges (resist tone changes at the center part of mid and long-ranges due to polymer cross linking at extreme doses).

width of a single shot that corresponds to 4 nm. Some line patterns were overwritten many times to overcome the allowed dose limit of the exposure system and achieve ultra-high line doses. Figure 3(a) shows microscopic images (top observation) of the line exposure calibration pattern after cleavage and before development. It can be noticed that resist's color slightly changes at extreme doses.

3.2. High contrast development in cold condition

In order to apply the threshold model and neglect developer effects, the development process should be characterized by a high contrast; which indicates that the developer has a rather digital behavior and stops dissolving the exposed resist at an equi-dose surface with a certain threshold dose value.[28] Modern development processes usually utilize strong developers with high contrasts. However, very high contrast development processes achieved by cold development for short time were recently reported.[29] Hence, a more accurate representation of the LSF can be obtained by introducing a similar development process to EDD extraction. Thus, the line exposure pattern was developed in ZED-N50 at −10 °C for 10 s. followed by two rinse steps in isopropyl-alcohol (IPA) at −10 °C and 20 °C for 10 s. in each step. Figure 3(b) shows microscopic images (top observation) of the line exposure calibration pattern after development. Half-width measurements were performed by cross-sectional SEM observation. Figure 4 shows SEM image samples of line half-width observation at resist's top and bottom at different scattering ranges. It can be noticed that resist tone changes for extreme doses at the center part due to polymer cross linking.[30] This effect is also encountered in literature for the point exposure method.[24]

3.3. LSF fitting

Figure 5 shows Monte-Carlo simulation of the PSF at the top and bottom surfaces of the resist. A layer stack of 700 nm thick ZEP, 220 nm thick top Si, 3 μm thick SiO_2, and 500 μm thick bulk Si substrate is used for the simulation. It can be noticed

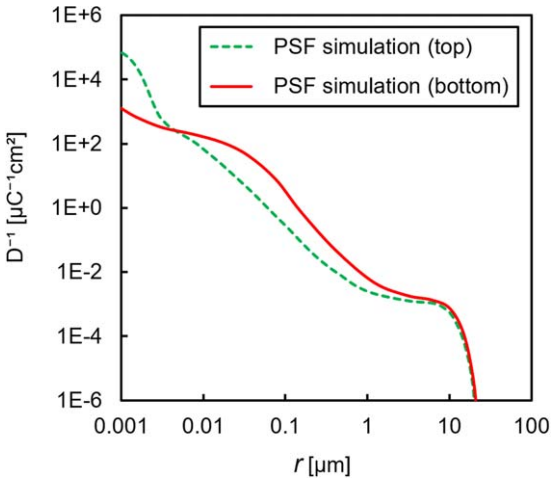

Fig. 5. (Color online) Monte-Carlo simulation of the PSF at the top and bottom resist surfaces.

that the PSF at the top is significantly different from that at the bottom. This is mainly caused by the different forward-scattering and backscattering effects in short- and mid-ranges, respectively, at different resist depths. In short-range, beam broadening increases with the resist depth. In addition, mid-range scattering effects are more pronounced near the bottom surface. For the sake of comparison, LSF measurement was performed at both the top and bottom surfaces and accurate measurement of resist half-widths was achieved by pixel counting in SEM images of the calibration pattern lines. LSF was obtained by plotting the inverse dose of the exposed lines against their corresponding measured half-width as shown in Fig. 6. The results agreed well with the previous argument.

The application of this work is dry etching of Si waveguide patterns, where vertical resist sidewalls are required to improve waveguide's etching conditions. Therefore, the controlled CD

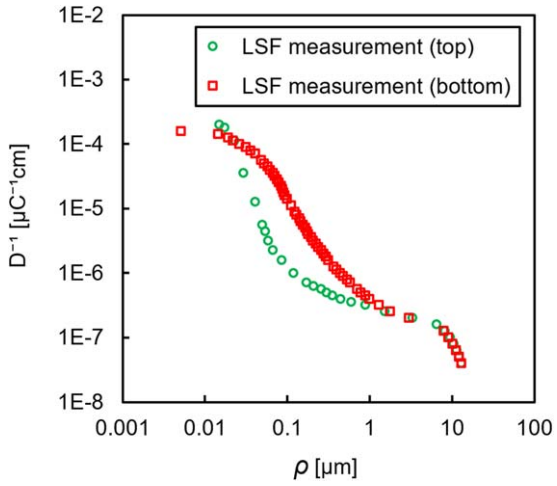

Fig. 6. (Color online) Measured LSFs at the top and bottom resist surfaces.

was decided to be the bottom resist width to reduce lateral development and achieve almost vertical sidewalls. Figures 7(a)–7(c) show the measured LSF distribution at the bottom together with a two, three, and four-Gaussian fitting, in addition to the corresponding relative error function. Due to the large energy span on the logarithmic *y*-axis, the error function was expressed by dividing the fitted value by the corresponding measured value, rather than subtracting. It is clear that a significant amount of energy density is located in the mid-range between $r \approx 0.1\,\mu$m to $r \approx 1$. Mid-range energy densities can be described as the distribution of energy at intermediate distances between the center and the tail of the electron beam, which results mainly from near-backscattering. Such energy densities were not appropriately modeled using a 2-Gaussian model or even a 3-Gaussian one as shown in Figs. 7(a) and 7(b), respectively, where fitting error peaks exist. However, mid-range energy density could be modeled accurately by a 4-Gaussian model that uses two Gaussian functions to represent near-mid-range and far-mid-range energy densities as shown in Fig. 7(c). Thus, the minimum fitting peak was reduced from -95.3% and -75.5% to -18.2% for the two, three, and four-Gaussian, respectively. The 3-Gaussian model has been commonly used in literature to model short, mid, and long-range scattering effects,[31] however, 4-Gaussian fitting was used in this work as the used PEC software[21] allows beam modeling with up to four Gaussians. Four-Gaussian modeling of the radial EDD is represented by the following equation:

$$\frac{D}{D_0} = \frac{1}{\pi(1+\eta+\upsilon_1+\upsilon_2)} \times \left\{ \frac{1}{\alpha^2} e^{-\frac{r^2}{\alpha^2}} + \frac{\eta}{\beta^2} e^{-\frac{r^2}{\beta^2}} + \frac{\upsilon_1}{{\gamma_1}^2} e^{-\frac{r^2}{{\gamma_1}^2}} + \frac{\upsilon_2}{{\gamma_2}^2} e^{-\frac{r^2}{{\gamma_2}^2}} \right\}, \quad (1)$$

where D/D_o is the dose intensity function, r is the radial distance, η, υ_1 and υ_2 are the scaling ratios for long-range, near and far-mid-range scattering, respectively, while α, β, γ_1 and γ_2 are the short-range, long-range, near and far-mid-range scattering parameters, respectively.

However, in order to obtain EDD for an infinitely long line, the beam's radial energy distribution is integrated along that line to yield the following LSF equation:

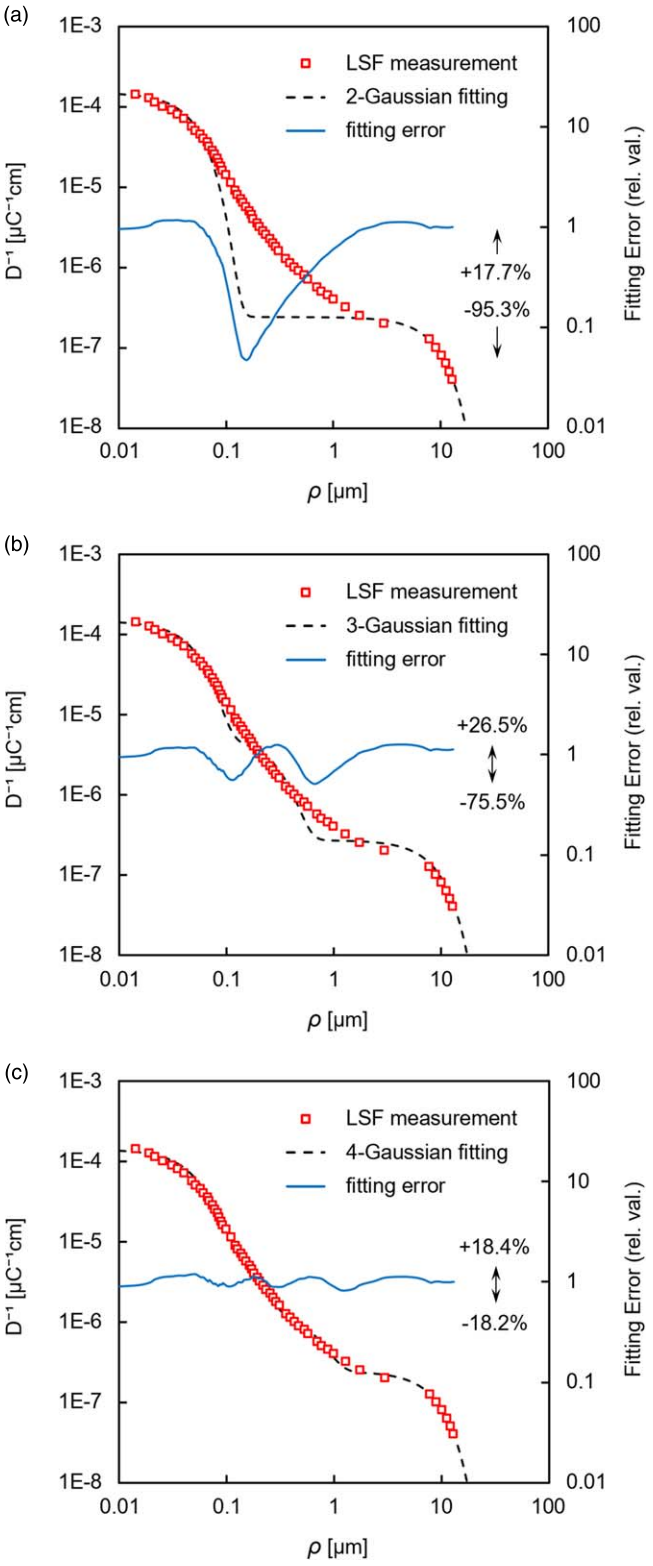

Fig. 7. (Color online) LSF measurement (squares) with fitting (dashed) and fitting relative error (solid) using (a) 2-Gaussians, (b) 3-Gaussians, and (c) 4-Gaussians.

$$\frac{D}{D_0} = \frac{1}{\sqrt{\pi}(1+\eta+\upsilon_1+\upsilon_2)} \times \left\{ \frac{1}{\alpha} e^{-\frac{\rho^2}{\alpha^2}} + \frac{\eta}{\beta} e^{-\frac{\rho^2}{\beta^2}} + \frac{\upsilon_1}{\gamma_1} e^{-\frac{\rho^2}{{\gamma_1}^2}} + \frac{\upsilon_2}{\gamma_2} e^{-\frac{\rho^2}{{\gamma_2}^2}} \right\}, \quad (2)$$

Table I. Extracted 4-Gaussian fitting parameters of the bottom LSF.

Parameter	Value	Dimension
α	52.5	nm
γ_1	155	nm
γ_2	655	nm
β	9.665	μm
υ_1	0.290	—
υ_2	0.120	—
η	0.355	—

where ρ is the lateral distance from the exposure line. LSF fitting to Eq. (2) in Fig. 7(c) was performed by a dedicated software code due to the large number of parameters involved. A conventional direct search algorithm was used with a repeatedly narrowing search grid to obtain the least squares error with enough accuracy. It should be noted that the sum of squares of errors was performed for the logarithm of the inverse doses rather than the absolute value in order to fit short, mid, and long-range energy densities equally. Table I shows the extracted 4-Gaussian parameters. The deposited radial EDD could be reconstructed from the extracted LSF by substituting in Eq. (1) with the obtained fitting parameters.

Monte-Carlo simulation of PSF at resist's bottom shown in Fig. 5 was estimated using a high accuracy commercial software[20] for the sake of comparison with the experimentally extracted one. For Gaussian beam systems, the radial EDD function that includes resist responses to actual process conditions is usually called the effective PSF (eff. PSF).[32] Such effective PSF, also called the total process function, is usually modeled by introducing a Gaussian process blur to the simulated PSF by 2D convolution.[20] The process blur itself can be simulated[33] or experimentally extracted.[34] It was found that a 40 nm process blur applied to the simulated PSF by Monte-Carlo leads to an effective PSF with a short-range scattering parameter α value of 52.5 nm. This value was the same as the experimentally extracted one in Table I, hence, 40 nm blur was used for comparing Monte-Carlo method to our proposed one. Figure 8 shows the simulated PSF by Monte-Carlo method, the calculated effective PSF assuming a 40 nm process blur, and the experimentally extracted effective PSF by parameter substitution from Table I in Eq. (2). It can be noticed that the calculated and experimentally extracted effective PSFs are similar in the short and mid-ranges, however, the long-range energy densities where $r > 1\ \mu$m are significantly lower for the experimentally extracted one.

4. Dose modulation PEC

4.1. Pattern development

In order to qualitatively verify this interesting finding, dose modulation PEC was performed by a commercial software[21] using both the simulated and experimentally-extracted EDDs. The software algorithm is based on the transform method which uses deconvolution. However, it reduces computational time by splitting the calculation into correction related and pattern related steps. Thus, the grid size is spatially independent from the pattern and can be as coarse as needed for correction. Pattern dimensions are maintained and data reduction is not needed in this algorithm. A minimum grid size of 40 nm was decided for the pattern, while minimum and maximum relative doses were 0.348 and 3.367, respectively. The modulated doses were quantized by the software to 229 (<256) different shot ranks to be exposed by the EBL system in each exposure field. Increasing the number of shot ranks is known to improve the algorithm's resolution and accuracy.

Figures 9(a)–9(c) show pattern development conditions at various doses with three different processes: without PEC by constant dosage, with the conventional PEC process by Monte-Carlo-simulation, and with the proposed PEC process by LSF extraction. EDDs shown in Fig. 8 for both PEC techniques were used for this experiment. The pattern used in each process was a 500 nm waveguide with 1 μm trench tapered to a 5 μm trench SSC. Resist clearance conditions at various doses were observed by an optical microscope for both 1 and 5 μm trench-width areas. Chip and exposure conditions were the same as those used in LSF extraction, however, development is performed with ZED-N50 at 20 °C for 30 s followed by 20 °C rinse in IPA for 30 s. Such conventional room temperature development process yields higher resist sensitivity with lower clearance dose. Hence, less exposure time can be achieved while having a contrast high enough for dry etching applications.

Figure 9(a) shows that both 1 and 5 μm trench-width areas are cleared at different doses without PEC. Due to proximity effects, the 1 μm trench-width area needs an additional

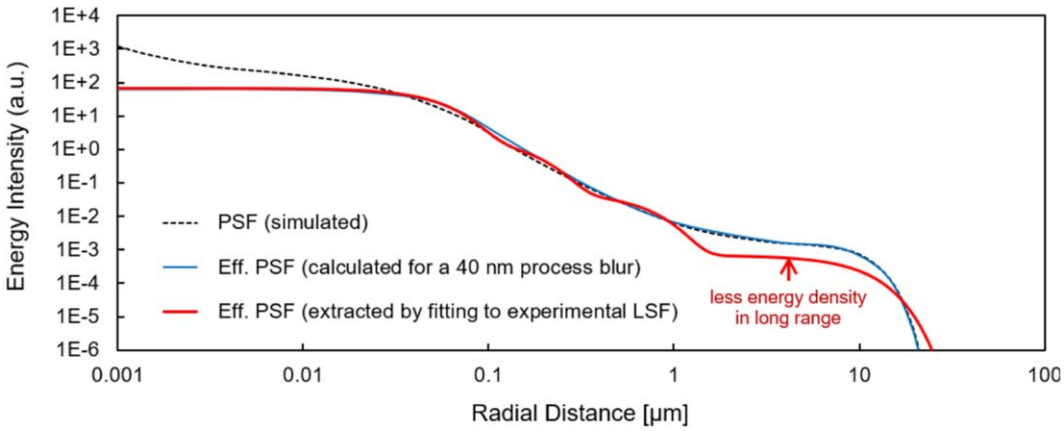

Fig. 8. (Color online) Comparison between the calculated PSF by Monte-Carlo method (dotted), the effective PSF calculated from Monte-Carlo simulation method assuming a 40 nm process blur (blue), and the effective PSF experimentally extracted from LSF fitting (red).

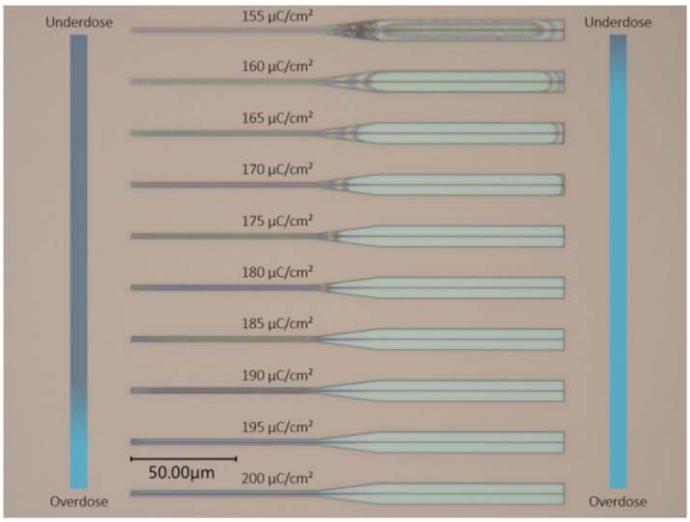

(a)

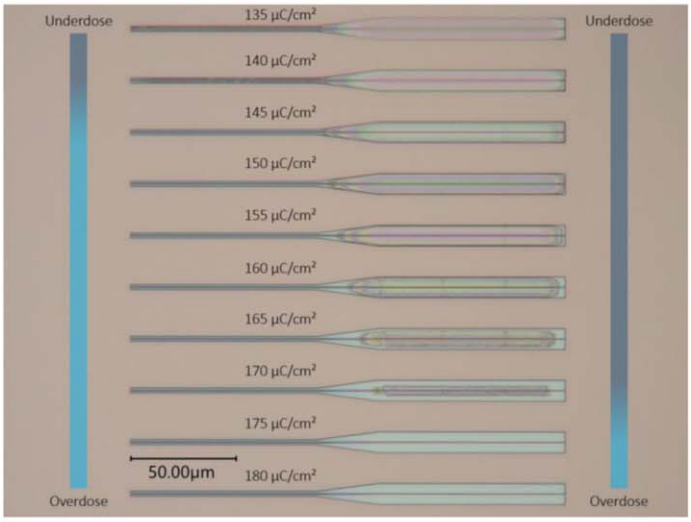

(b)

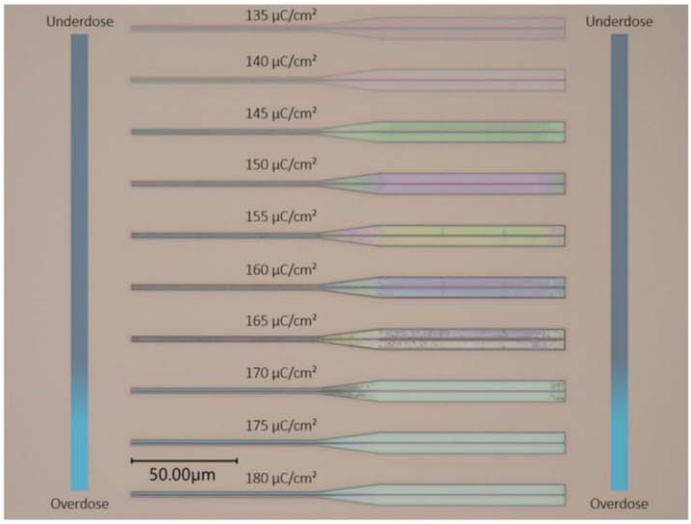

(c)

Fig. 9. (Color online) Si waveguide line patterns with 1 and 5 μm side-cladding trench widths fabricated with (a) a constant dosage, (b) the conventional Monte-Carlo PEC method, and (c) the improved LSF extraction PEC method (color scales are inserted for reference).

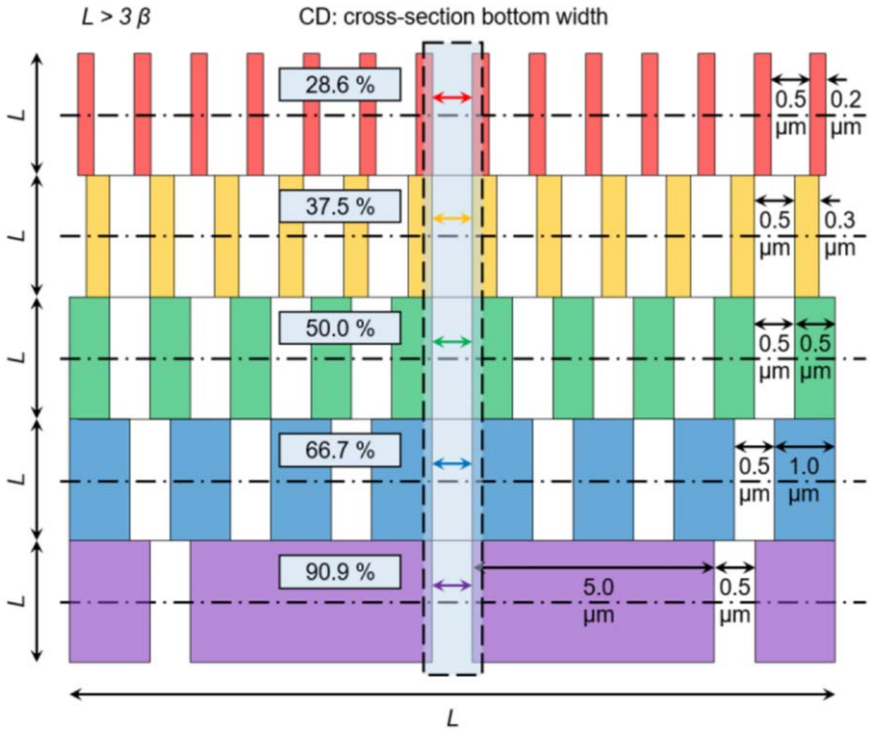

Fig. 10. (Color online) Schematic top-view of the tower pattern (dimensions are not to scale).

~21% (±3%) more dosage than the 5 μm trench-width area to be cleared. Moreover, the conventional PEC process by Monte-Carlo-simulation also showed a significant error in proximity correction. Figure 9(b) shows that the 1 μm trench-width area needs ~17% (±3%) less dosage than the 5 μm trench-width area to be cleared completely, which implies overestimation of proximity effects for that process. However, the proposed PEC process by LSF extraction shows better matching between the development conditions of both 1 and 5 μm trench-width areas. Figure 9(c) shows that clearance doses of both areas are very close. This verifies the result obtained from Fig. 8 where less proximity effect was expected in the long-range by experiment, and hence, higher energy densities actually exist in the short-range.

4.2. Linewidth uniformity

To obtain a quantitative description of linewidth uniformity with pattern area density, a tower pattern shown in Fig. 10 was exposed and developed using the same process conditions. Figures 11(a) and 11(b) show the extracted tower diagram which describes the developed widths of periodic 500 nm waveguides at different pattern densities without and with the proposed PEC process, respectively. Pattern area densities were 28.6%, 37.5%, 50.0%, 66.7%, and 90.9%, which correspond to periodic patterns of 500 nm width lines with 200 nm, 300 nm, 500 nm, 1 μm, and 5 μm gaps, respectively. The measured CD values were obtained by SEM observation of resist's bottom width after cleavage.

Figures 11(a) and 11(b) clearly show that a single-dose (without PEC) could not even develop all pattern area densities, while the proposed PEC process could develop the pattern with high CD uniformity near a base dose. On the other hand, it was confirmed by Figs. 11(b) and 11(c) that the proposed PEC method could achieve a small linewidth variation of less than ~12 nm (~2.4%) within the tested pattern area density range at the base dose of 170 μC cm^{-2}. For actual device fabrication, a fixed width bias of 6 nm should be subtracted, and etching-induced shrinkage should be added to the exposed pattern widths. Thus, compensation of both effects can keep CD error within ±6 nm. This width bias can be applied to the whole pattern automatically by the utilized software. A dose margin of 5 μC cm^{-2} around the base dose yields CD deviation of ±10 nm, which is a commonly encountered tolerance in some EBL and DUV lithography processes.[10] Such a dose margin is much higher than the error caused by EBL current fluctuations. This reported CD accuracy was also limited by our manual spin coating and development processes and may be improved by using automated fabrication steps. However, a clear and significant improvement could be observed.

In order to test the proposed PEC process, a single-mode 500 nm SOI wire waveguide propagation loss measurement pattern with different waveguide lengths was fabricated using both a fixed dose and the proposed dose modulation PEC process. Figure 12 shows a schematic of dose modulation PEC applied to the propagation loss measurement pattern using a commercial software[28] with the previously mentioned PEC settings. Values in image insets show local doses as a ratio of the base dose. Figures 13(a) and 13(b) show cross-sectional SEM images of Si waveguides fabricated by inductive coupled plasma reactive ion etching (ICP-RIE) without and with trench width modulation, by a fixed dose and dose modulation PEC, respectively. It can be seen that the waveguide sidewalls are more vertical by using PEC as the etching mask sidewalls themselves became more vertical. Resist masks with vertical sidewalls promote etching anisotropy by limiting resist undercuts caused by pattern over-development.

4.3. Si waveguide propagation loss

Propagation loss measurement of the single-mode waveguide was conducted using 1530–1610 nm amplified spontaneous emission (ASE) light source injected to a lensed polarization

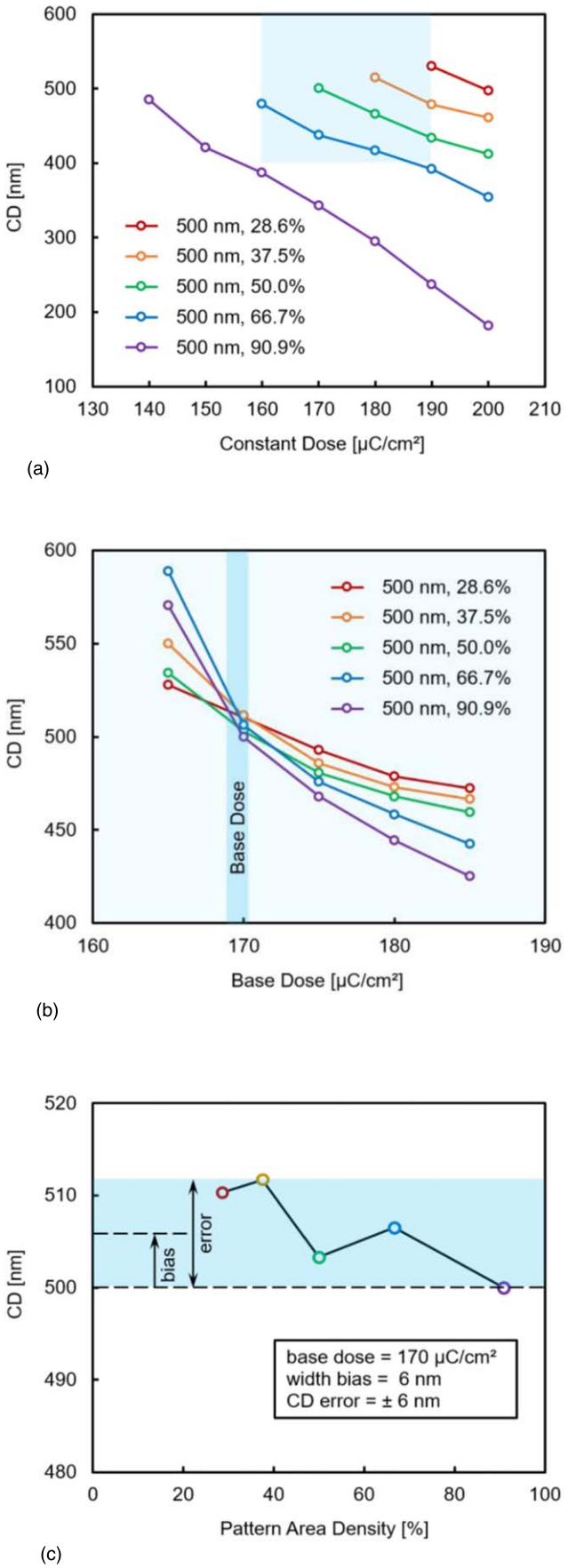

Fig. 11. (Color online) CD variation with dosage and pattern area density with (a) constant doses, (b) dose modulation PEC with the improved LSF extraction method, and (c) pattern area density at a base dose of 170 μC cm^{-2}.

maintaining fiber (PMF) through a polarizer. The lensed PMF fiber was adjusted such that the optical mode injected into the chip was polarized as transverse electric (TE). The mode was coupled to the chip by an input SSC, propagated through the waveguides until the output SSC, and then was coupled to a lensed single mode fiber. The output signal was measured by an optical power meter.

Figure 14 shows insertion losses versus waveguides lengths. Propagation loss was found to be reduced from 3.2 to 2.4 dB cm^{-1}. Such reduction of propagation loss might be attributed to a reduction in sidewall roughness due to changes in fabrication conditions after applying PEC. One possibility is that achieving vertical resist sidewalls might have reduced the severity of mask erosion from the side, and hence, reduced the transferred sidewall roughness to Si. Another possibility is that the narrower trench width resulted in a reduction in sidewall roughness by ICP-RIE. Generally, roughness reduction might be due to a combination of both possibilities. Thus, trench width modulation (1 μm width instead of 5 μm) allowed by PEC not only reduced exposure time but also could reduce waveguide propagation loss.

5. Discussion

By comparing the simulated and extracted effective PSF distributions in Fig. 8 and their corresponding PEC results in Fig. 9, the large influence of the assumed EDD on PEC process accuracy can be deduced. It can be seen that a change which seems to be small in EDD function can significantly affect development conditions of the proximity effect corrected pattern. In Fig. 9(a), due to the proximity effect, resist residuals are observed at pattern corners (where pattern area density is lower) even at rather higher doses. In contrast, Fig. 9(b) shows that the resist starts to resolve from pattern corners at base dose of 160 μC cm^{-2}, due to the overestimation of proximity effect using the conventional Monte-Carlo-based PEC process. Resist residuals can be seen along the waveguide pattern (where pattern area density is higher) even at a higher base dose of 170 μC cm^{-2}, indicating lower contrast of the deposited energy profile at the bottom. Such lower contrast reduces the verticality of resist sidewalls after development. However, in Fig. 9(c), resist residuals in the whole exposed area (where pattern area density is varying) look almost uniform as the base dose increases. The resist was immediately resolved at a base dose of 170 μC cm^{-2}. This demonstrates the effectiveness of the proposed PEC process as high contrast was uniformly obtained along the waveguide. As a result, roughness after etching is thought to be improved. Results in Fig. 9(c) also suggest that the proposed LSF calibration with cold development after cleavage succeeded in extracting the effective PSF accurately even at the short-range.

The differences between the conventional and proposed calibration methods shown in both Figs. 8 and 9 might be caused by various reasons. Possibly, some parameters and/or physics used in Monte-Carlo scattering calculations might have been empirically extracted from data in the literature that was not enough to fully and accurately describe scattering effects in our material stack. Regardless of such reasons, the proposed experimental calibration method succeeded to accurately achieve PEC at a single-base dose.

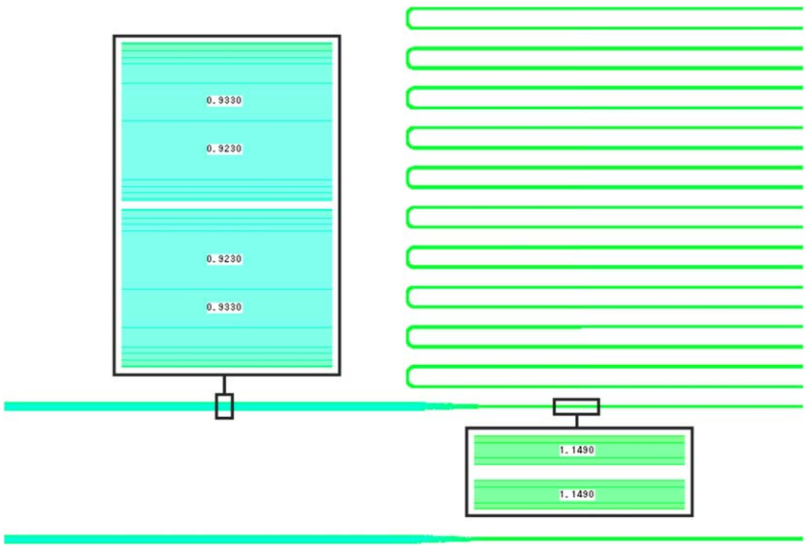

Fig. 12. (Color online) Schematic (partial view) of single-mode waveguide propagation loss measurement pattern with the proposed dose modulation PEC applied (image insets show relative dose values).

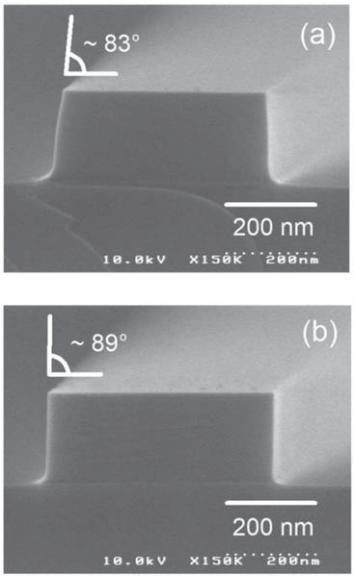

Fig. 13. Cross-sectional SEM images of 500 nm width waveguides (a) with 5 μm trench (by a fixed dose), and (b) with 1 μm trench width (by dose modulation PEC).

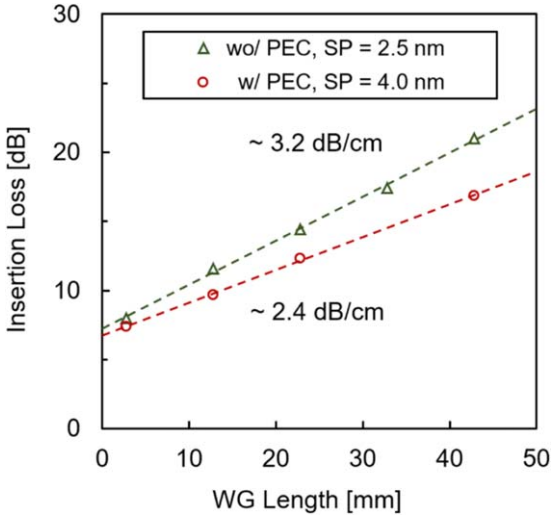

Fig. 14. (Color online) 500 × 220 nm Si wire waveguide propagation loss with 5 μm trench (wo/PEC) and 1 μm trench (w/PEC).

Future work is needed to study the effect of the development process contrast on LSF calibration. In addition, LSF extraction for different resist types and thicknesses or at different electron acceleration voltages may help in formulating a better understanding of the deviation between the Monte-Carlo simulation and experimental result.

6. Conclusions

In this work, an improved calibration process for accurate extraction of electron beam EDD was proposed and experimentally validated by applying dose modulation PEC to Si photonics waveguides patterns. The calibration process is based on an improved LSF method by cold development of calibration lines after cleavage to allow better extraction of short-range scattering information at the resist bottom. LSF data was fitted to a 4-Gaussian model to accurately model near-mid-range and far-mid-range energy densities by two Gaussian functions.

Experimental results showed fewer proximity effects in the long-range compared to the conventional Monte-Carlo-based technique. Microscopic images confirmed the previous finding as the proposed calibration method could achieve better development conditions at a single base dose. Moreover, the tower diagram showed high CD uniformity of ±6 nm (with a fixed bias of 6 nm) for 500 nm waveguide patterns with different pattern area densities. This CD tolerance corresponds to as low as 10% inaccuracy of the grid spacing in a 50 GHz DWDM ITU grid system with ~20 μm diameter ring-resonator filters. Using the proposed PEC process, single-mode 500 × 220 nm Si wire waveguide sidewall angle was improved from 83° to 89°. Achieving vertical sidewalls with angles >88° is critical for some Si photonics devices especially for TM polarization. It also helps to achieve a good match between device simulation and measurement generally. Propagation loss for the TE-like mode was also reduced from 3.2 to 2.4 dB cm^{-1} due to the improved resist mask shape. Further improvement of CD accuracy and waveguide propagation loss might be achieved

by introducing automated fabrication processes and sidewall roughness smoothing techniques, respectively.

Acknowledgments

The authors would like to thank to Dr. Satoshi Shimizu of GenISys for experimental help and discussion. This work was financially supported by New Energy and Industrial Technology Development Organization (NEDO), JST-ACCEL (JPMJAC1603), JST-CREST (JPMJCR15N16), JSPS KAKENHI Grant Nos. (#16H06082, #17H03247).

ORCID iDs

Moataz Eissa https://orcid.org/0000-0002-4339-2724
Yasuyuki Miyamoto https://orcid.org/0000-0002-2676-7264
Nobuhiko Nishiyama https://orcid.org/0000-0001-8288-6690

1) Y. Arakawa, T. Nakamura, Y. Urino, and T. Fujita, IEEE Commun. Mag. **51**, 72 (2004).
2) R. Soref, IEEE J. Sel. Top. Quantum Electron. **12**, 1678 (2006).
3) A. Ghiasi, Opt. Express **23**, 2085 (2015).
4) T. Barwicz et al., J. Opt. Netw. **6**, 63 (2007).
5) V. J. Sorger, N. D. Lanzillotti-Kimura, R. M. Ma, and X. Zhang, Nanophotonics **1**, 17 (2012).
6) A. Prinzen, M. Waldow, and H. Kurz, Opt. Express **21**, 17212 (2013).
7) X. Wang, W. Shi, M. Hochberg, K. Adam, E. Schelew, J. F. Young, N. A. F. Jaeger, and L. Chrostowski, 9th Int. Conf. on Group IV Phot. (GFP), 2012, p. 288.
8) D. Dai and M. Zhang, Opt. Express **23**, 32452 (2015).
9) R. J. Bojko, J. Li, L. He, T. Baehr-Jones, and M. Hochberg, J. Vac. Sci. Technol. B **29**, 06F309 (2011).
10) D. Xu, J. H. Schmid, G. T. Reed, G. Z. Mashanovich, D. J. Thomson, M. Nedeljkovic, X. Chen, D. Van Thourhout, S. Keyvaninia, and S. K. Selvaraja, IEEE J. Sel. Top. Quantum Electron. **20**, 8100217 (2014).
11) Y. Tanushi et al., 10th Int. Conf. on Group IV Phot. (GFP), 2013, p. 105.
12) L. Pain, S. Tedesco, and C. Constancias, C. R. Phys. **7**, 910 (2006).
13) V. R. Manfrinato, L. Zhang, D. Su, H. Duan, R. G. Hobbs, E. A. Stach, and K. K. Berggren, Nano Lett. **13**, 1555 (2013).
14) T. H. P. Chang, J. Vac. Sci. Technol. **12**, 1271 (1975).
15) L. D. Jackel, R. E. Howard, P. M. Mankiewich, H. G. Craighead, and R. W. Epworth, Appl. Phys. Lett. **45**, 698 (1984).
16) A. H. K. Park, H. Shoman, M. Ma, S. Shekhar, and L. Chrostowski, Opt. Express **27**, 6147 (2019).
17) E. Seo, B. K. Choi, and O. Kim, Microelectron. Eng. **53**, 305 (2000).
18) Y. Atsumi, N. Taksatorn, N. Nishiyama, Y. Miyamoto, and S. Arai, Jpn. J. Appl. Phys. **53**, 06JB04 (2014).
19) M. Asteiner, C. Schlemmer, P. Speckbacher, and K. E. Hoffmann, J. Vac. Sci. Technol. B **34**, 041601 (2016).
20) TRACER, Electron scattering and process effects quantification software developed and distributed by GenISys GmbH (www.genisys-gmbh.com/tracer.html).
21) BEAMER, Electron-beam lithography software developed and distributed by GenISys GmbH (www.genisys-gmbh.com/beamer.html).
22) A. R. Neureuther, D. F. Kyser, and C. H. Ting, IEEE Trans. Electron Devices **26**, 686 (1979).
23) L. E. Ocola and A. Stein, J. Vac. Sci. Technol. B **24**, 3061 (2006).
24) S. A. Rishton and D. P. Kern, J. Vac. Sci. Technol. B **5**, 135 (1987).
25) S. Aya, K. Kise, H. Yabe, and K. Marumoto, Jpn. J. Appl. Phys. **35**, 1929 (1996).
26) Q. Dai, S. Y. Lee, S. H. Lee, B. G. Kim, and H. K. Cho, Microelectron. Eng. **88**, 3054 (2011).
27) J. C. H. Phang and H. Ahmed, J. Vac. Sci. Technol. **16**, 1754 (1979).
28) R. F. Herzog, J. S. Greeneich, T. E. Everhart, and T. Van Duzer, IEEE Trans. Electron Devices **19**, 635 (1972).
29) L. Y. M. Tobing, L. Tjahjana, and D. H. Zhang, J. Vac. Sci. Technol. B **30**, 051601 (2012).
30) B. Cord, J. Lutkenhaus, and K. K. Berggren, J. Vac. Sci. Technol. B **25**, 2013 (2007).
31) S. J. Wind, M. G. Rosenfield, G. Pepper, W. W. Molzen, and P. D. Gerber, J. Vac. Sci. Technol. B **7**, 1507 (1989).
32) J. Zhou and X. Yang, J. Vac. Sci. Technol. B **24**, 1202 (2006).
33) B. Cord, J. Yang, and H. Duan, J. Vac. Sci. Technol. B **27**, 2616 (2009).
34) N. Unal, M. D. B. Charlton, Y. Wang, U. Waizmann, T. Reindl, and U. Hofmann, Microelectron. Eng. **88**, 2158 (2011).